Understanding the dwell-fatigue-damage mechanism of powder metallurgy Ti-6Al-4V alloys fabricated by hot isostatic pressing

Yaoxin Huo[a], Ruipeng Guo[a,*], Junwei Qiao[a], Lei Xu[b,*], Rui Yang[b], and Peter K. Liaw[c]

[a]*College of Materials Science and Engineering, Taiyuan University of Technology, Taiyuan 030024, China*

[b]*Institute of Metal Research, Chinese Academy of Sciences, Shenyang 110016, China*

[c] *Department of Materials Science and Engineering, The University of Tennessee, 37996–2200 Knoxville, TN, USA*

Corresponding authors. E-mail: grp88620@163.com (R. Guo); lxu@imr.ac.cn (L. Xu).

Abstract:

Dwell fatigue of titanium alloys used in aeroengine components has threatened the reliability of aircraft for decades. Powder metallurgy (PM) through hot-isostatic pressing (HIPing) can fabricate titanium-alloy components with complex structures, and the mechanical properties are close to wrought alloys. Unfortunately, the dwell-fatigue behavior of the as-HIPed titanium alloy powder components has not been reported in previous studies. The present work firstly investigates the effects of the peak stress (σ_p) and stress ratio (R) on the dwell-fatigue behavior and damage mechanism of the as-HIPed Ti-6Al-4V powder. With increasing σ_p, the dwell-fatigue lives (N_{LCDF}) decrease, but the dwell debit increases. The lowest N_{LCDF} has been obtained at R = 0.1. With increasing R, the fatigue behavior of dwell fatigue is approaching to creep fatigue. When R is negative, the introduction of a lower reverse stress reduces the cumulated max. plastic strain, resulting in increasing N_{LCDF}.

Moreover, a crack-initiation and propagation model based on soft-hard grain pairs is proposed to describe the dwell-fatigue mechanism. In addition, the dwell debit of PM Ti-6Al-4V alloys is similar to or even lower than that of wrought alloys. Improving the microstructure homogeneity of the material may be the key to further reducing the dwell effect.

Keywords: Titanium alloys; Dwell effect; Fatigue damage; Powder metallurgy; Hot isostatic pressing

1. Introduction

Titanium alloys are promising structural materials for the application in the aeroengine industry due to their high strength-to-weight ratio, corrosion resistance, and excellent mechanical properties [1]. At present, titanium alloys have become the main materials for the manufacture of safety-critical components, such as compressor discs, fan discs, and blades in turbofan engines. Traditional safety-design criteria are based on general fatigue tests (with triangular or sine waves) to predict fatigue life. [2]. Unfortunately, owing to the complex stress conditions (take off-cruise-landing) of the actual service of the aircraft, the titanium alloy components need to withstand long periods of high stress retention and may fail prematurely, resulting in fatigue life significantly lower than expected. This phenomenon, known as a dwell effect, was first discovered from the failure in RR RB211 engine titanium disks in the 1970s [3-5], which seriously threatens the reliability of aeroengine components. Compared with general fatigue, the fatigue life of components under dwell fatigue (with trapezoidal wave) decreases by an order of magnitude or more [6, 7].

Recently, dwell fatigue has attracted wide attentions due to its concealment and destructiveness. The main feature of the dwell-fatigue-fracture morphology is the formation of facets for titanium alloys, which is considered to be the origin of a crack-initiation site [3]. It is generally believed that the formation of facets under dwell fatigue is caused by slip activity, which is the key to revealing the dwell effect [5]. Basal slip is considered to be more likely to trigger crack nucleation than prism slip. Many studies have shown that the crack-initiation facets that cause the main cracks are formed at or very close to the basal planes [8-10]. However, Bridier *et al.*[11] have also reported the formation of prism facets at the crack-initiation sites. Lavogiez *et al.*[12] and Hémery *et al.*[13] demonstrated that cracks may be also formed at the (0001) twist boundary in Ti-6Al-4V. However, it is still unclear how the local stress concentration leads to crack nucleation at the twist boundary and whether the main crack initiates in such a microstructure configuration.

Evans and Bache [3, 14] proposed the soft and hard grains to explain the mechanism of crack initiation in dwell fatigue. They assumed a microstructural configuration consisting of a grain (soft grain) suitable for basal or prism slip activation and a grain (hard grain) unsuitable for slip orientation. The slip in soft grains leads to dislocation pileups at hard grain boundaries and provides a sufficient shear stress on the basal plane of hard grains, thus inducing the nucleation of the basal or near basal facets. This particular microstructure configuration has been proved by many experiments and widely accepted to reveal the dwell effect of titanium alloys [15-17]. On the macroscopic scale, the hard grains are likely to correspond to the

(0001) microtexture regions. Qiu *et al.*[18] have shown that the dwell effect increases with increasing the microtexture strength. In addition, Bache *et a*l.[19] have shown that the compressor disks will show a stronger dwell effect than the forging rod, which may be due to the strong microtexture caused by the die-forging process.

Compared with steels and aluminum alloys, titanium alloys are usually hard to machine. The buy-to-fly ratio of titanium-alloy components produced by conventional manufacturing processes is very high, and the material loss may be more than 80% due to the geometric complexity of aeroengine components [20]. Alternatively, powder-metallurgy (PM) processes have been used to reduce production costs through near-net-shape forming [21, 22]. However, the retained porosity of PM components seriously affects their fatigue performance and restricts their application in the aviation industry. The PM through a hot-isostatic-pressing (HIP) route can produce large components with complex geometries, and the corresponding microstructure is fine and homogeneous [23]. Previous studies have reported that the as-HIPed PM titanium alloys are close to a full density, and their static mechanical properties are comparable to even better than wrought materials [24-26]. Cheng *et al.* [27] revealed that the residual pores in the as-HIPed powder compacts have no obvious effect on the high-cycle fatigue life. Guo *et al*.[28] found that the high-cycle fatigue strength of titanium-alloy-powder compacts can be better than wrought alloys by in-situ globalization during the HIP process. Lastly, Sun *et al*. [29] showed that the defects do not reduce the dwell-fatigue life due to the plastic deformation caused by the dwell dominates the dwell-fatigue life rather than defects under the high stress level

approaching to the yield stress. Therefore, a small amount of residual porosity (< 0.1vol.%, volume fraction) may not affect the dwell-fatigue property of as-HIPed powder compacts. To the best knowledge of the authors, there are limited literatures on the dwell-fatigue behavior of PM titanium alloys. This study aims to investigate the effect of external loading conditions on the dwell-fatigue life of as-HIPed Ti-6Al-4V powder compacts. The fatigue-crack initiation and propagation mechanisms were discussed, based on the characterization of microstructures and fracture surfaces.

2. Materials and methods

2.1. Materials

The material used in this study was a PM Ti-6Al-4V alloy prepared from an HIP route. The chemical compositions (weight percentage, wt.%) of powder compacts were 6.05Al, 4.04V, 0.05Fe, 0.03Si, 0.02C, 0.12O, 0.003N, 0.002H, and balance Ti. The HIP process has been reported in detail elsewhere [30]. The microstructure and tensile properties of Ti-6Al-4V powder compacts are shown in Fig. 1. It can be seen that the microstructure was fine and homogeneous and made up of about a 94% lamellar and equiaxed primary α phase (α_p, black) and 6% β phase (white). The grain size of the equiaxed α phase was about 6.2 μm, and the width of the lamellar α phase was about 3.3 μm. The yield strength (σ_y), tensile strength (σ_u), and elongation (δ) of Ti-6Al-4V powder compacts were 840 MPa, 915 MPa, and 14.9%, respectively.

2.2. Microstructural characterization

Microstructures of powder compacts were observed, using scanning electron microscopy (SEM, ZEISS Gemini 300) equipped with an electron backscatter

diffraction (EBSD) system and transmission electron microscopy (TEM, TECNAI G^2 F30). The samples for SEM observations were ground to 3,000 meshes by sandpaper, polished by 0.02 μm silica suspension and chemically etched by Kroll's reagent (2% HF + 4% HNO_3). The EBSD samples were ground, polished, and electrolytically etched, using a reagent of 59% CH_3OH + 35% $C_4H_{10}O$ + 6% $HClO_4$ (vol.%) at -30 ℃ and a current density of 1 mA/cm^2 for about 45 s. The EBSD results were analyzed by a TSL OIM 7.0 software. The TEM foils were cut from the longitudinal section of the fatigue-fracture crack initiation region along the loading direction, and prepared by the ion-beam thinning technique.

2.3. Mechanical tests

Fatigue and tensile testing specimens were cut from Ti-6Al-4V powder compacts with a diameter of 50 mm and a height of 200 mm by electrical discharge machining. The schematics of the tensile and fatigue specimens were shown in Fig. 2. Tensile tests were carried out on an INSTRON 5969 mechanical testing machine using the cylindrical specimens, 5 mm in diameter and 30 mm in gauge length. Fatigue tests were performed on a BISS UT-01-0025 servo hydraulic closed-loop testing system at ambient temperature using the cylindric specimens, 4 mm in diameter and 14 mm in gauge length. The low-cycle-fatigue (LCF) and low-cycle- dwell fatigue (LCDF) specimens were the same (Fig. 2b). The loading spectra were presented in Fig. 3. The LCF experiments were carried out, employing a triangular wave with a 0.5-s dwell, while the LCDF experiments were carried out, using a trapezoidal wave with a 120-s dwell. The loading and unloading time, was 1 s for both the LCF and LCDF tests.

Three different stress ratios (R, the ratio of minimum stress to maximum stress) of -0.1, 0.1, and 0.5, and the peak stresses (σ_p) of the $0.92\sigma_y$ (775 MPa), $0.95\sigma_y$ (800 MPa), and $0.98\sigma_y$ (825 MPa) were adopted for the LCF and LCDF tests, respectively. All the fracture surfaces of the failed fatigue specimens were examined by SEM.

3. Results

3.1. Effect of stress ratio on fatigue life

The LCDF lives in this study were evaluated, using a 120-s dwell, which has often been adopted as a more practical period for dwell-effect assessments [3]. The average LCDF lives of the as-HIPed Ti-6Al-4V under different R with the σ_p of 825 MPa were list in Table 1. When the R is 0.1, the average LCDF lives is the shortest, only 201 cycles. As the R increases from 0.1 to 0.5, the average LCDF lives increases significantly to 1,255 cycles. However, when the R changes from 0.1 to - 0.1, the average LCDF lives (874 cycles) is also longer than that when the R is 0.1. The R reflects the magnitude of the stress amplitude in the load spectra. For the LCF, it was usually believed that the larger the stress amplitude, the lower the fatigue life [31]. However, the correlation between the LCDF lives and the stress amplitude is not a simple linear relationship, which means that fatigue-damage mechanisms under the R of - 0.1, 0.1, and 0.5 may be different.

3.2. Effect of peak stress on fatigue life

Previous work found that the dwell effect occurred in the range of 0.65 - 1.05 yield strength [19]. In the present work, different σ_p (775, 800, and 825 MPa) were adopted to investigate the effect of σ_p on the dwell effect of the as-HIPed alloys. The

value of the dwell effect has been usually evaluated by the following formula:

$$\text{Dwell debit} = \frac{N_{LCDF}}{N_{LCF}} \quad (1)$$

where N_{LCDF} is the LCDF life, and N_{LCF} is the LCF life.

The loading conditions and related fatigue lives under the R of 0.1 were shown in Table 2. Figure 4a displays the fatigue lives and dwell debit under different σ_p. With increasing σ_p, both N_{LCF} and N_{LCDF} decrease. The σ_p only increases by 3%, and both N_{LCF} and N_{LCDF} are drastically reduced by 40% ~ 60%. It is notable that the dwell debit increases obviously with increasing σ_p. When the σ_p is 775 MPa, the dwell debit is 2.12. When the σ_p increases to 800 MPa and 825 MPa, the dwell debit rapidly increases to 6.37 and 7.93, respectively. It indicates that the dwell effect of the PM Ti-6Al-4V is very sensitive to the σ_p. Figure 4b depicts a comparison of the dwell debit between the PM Ti-6Al-4V alloy and other wrought titanium alloys [5, 12, 18, 29, 32-35]. It was found that the dwell-effect sensitivity of the PM Ti-6Al-4V is similar to or even weaker than that of wrought alloys, which may be attributed to the better microstructural homogeneity.

3.3. Fractography

Fractographic analysis was performed on all of the failed fatigue specimens with R = 0.1 to investigate the crack initiation and propagation behavior. The SEM images of LCF and LCDF specimens with σ_p of 775, 800, and 825 MPa are shown in Figs. 5-7, respectively. Typical radial patterns representing the crack-propagation regions were observed on the fracture surfaces of all LCF and LCDF specimens. These regions can be observed on low-magnification SEM images [Figs. 5-7(a, b, e, f)]. By

tracking this radial pattern back to its origin and discriminating the characteristics of the corresponding regions, the most probable crack-initiation sites can be obtained (indicated by the red dotted lines). It was found that in all LCF and LCDF specimens, these sites were located on the subsurface or interior. High-magnification SEM images of these crack-initiation regions were shown in Figs. 5-7(c,g). The specimens present the quasi-cleavage fracture mode under both LCF and LCDF conditions. Quasi-cleavage facets with smooth surfaces can be easily observed at the crack-initiation regions, which are considered to be the results of the gradual separation of the slip damage concentrated within a persistent planar slip band [3, 5, 14]. Some facets have the similar dimensions corresponding to the equiaxed α_p, while others are consistent with lamellar clusters formed from the lamellar α_p usually with similar orientation. The main difference for LCF and LCDF is that there is usually only one crack-initiation site on the fracture surfaces of each LCF specimens, while the LCDF specimens have a higher probability of multiple crack-initiation sites.

Fatigue striations near the crack-initiation regions of LCF and LCDF specimens were shown in Figs. 5-7(d, h). The fatigue-striation spacings are0.57, 0.66, and 1.3 μm for LCDF specimens, and 0.38, 0.46, and 0.78 μm for LCF specimens, respectively. Although the fatigue-striation spacing increases with increasing σ_p, the fatigue-striation spacing of LCDF specimens is much larger than that of LCF specimens at the same σ_p.

4. Discussion

4.1. Damage mechanisms of dwell fatigue

In Table 1, it can be seen that when R is positive, the N_{LCDF} increases with the increase of R from 0.1 to 0.5. When $R = -0.1$, the N_{LCDF} is also longer than that when $R = 0.1$. The cumulated max. plastic strain (ε_{cum}) versus N_{LCDF} under different R has been plotted in Fig. 8a. It can be seen that compared with $R = 0.1$, the maximum of ε_{cum} at $R = 0.5$ is lower, and the growth rate is slower. This is because the stress amplitude under this condition is relatively small, so that the grains under this case are not completely squeezed, and the damage mode is close to creep damage. Besides, the maximum and growth rate of ε_{cum} at $R = -0.1$ are also lower than those at $R = 0.1$. Bache [3] proved that if the stress redistribution model is correct, there may be significantly different fatigue responses for the load spectra (tension and compression) containing the reverse load. Although the stress amplitude is larger, the introduction of the reverse stress releases the dislocation accumulation in the grains to a certain extent, which is beneficial to lowering the local stress concentration, thereby reducing the accumulation of ε_{cum} and improving the N_{LCDF}.

The ε_{cum} - N_f of LCF and LCDF under different σ_p was shown in Fig. 8b. Obviously, the ε_{cum} of LCF and LCDF both increases fastest in the early stage, and the growth rate slows down with increasing N_f. It is also noted that the maximum ε_{cum} achieved by LCDF is higher than that of LCF under the same σ_p during the whole fatigue tests, leading to higher material damage and shorter fatigue life, which can be demonstrated by the fractographic analysis in Figs. 5-7. Compared with LCF, there are multiple crack-initiation sites on the fracture surfaces of failed LCDF specimens, and these crack-initiation sites are much rougher and have more quasi-cleavage facets.

Zeng *et al.* [35] found that slip is the main deformation form of the α_p phase in Ti-6Al-4V alloys, and crack initiation is triggered by the activated slip under LCDF. The dwell at the σ_p accelerates the activation of the relevant slip systems, making the initiation of microcracks easier, resulting in more crack-initiation sites and facets. In addition, the spacing of fatigue striations under the LCDF is larger than that under the LCF during the crack-propagation stage. After the crack initiation, the microcracks propagate more rapidly to form the main crack under the continuous dwell cycle, and eventually leads to fracture failure, which significantly shortens the fatigue life. To sum up, the dwell at the σ_p acts on the whole fatigue stage, not only promoting the crack initiation, but also accelerating the crack propagation. The ε_{cum} reflects the degree of material damage [12, 34]. It is expected that the lower degree of damage per unit cycle, the longer N_{LCDF}.

4.2. Crack-initiation and propagation mechanisms of dwell fatigue

In LCDF, the whole fatigue life includes crack-initiation and propagation stages. The mechanisms of these two stages are necessary for understanding the dwell effect. Previous studies show that the initiation of fatigue cracks is closely related to the strong slip bands [11, 36]. The activation of a slip band is mainly quantified by a critical resolved shear stress (CRSS) and Schmid factor, which depend on the crystal orientation relative to the loading direction. In α-titanium single crystals, the prism and basal <a> slip are the main slip modes, because the CRSS of the pyramidal <c + a> slip may be more than three times higher than the basal and prism <a> slip [37]. Moreover, the inhomogeneity of the microstructure and internal stress in practical

materials also affects the slip mode. Liu *et al.*[38] proved that the formation of fatigue cracks in a near α titanium alloy is closely related to the basal slip formed in the early stage of cyclic loading. Fan *et al*. [39] showed that the basal slip is the main slip mode in a $\alpha + \beta$ titanium alloy in quasi-in-situ fatigue experiments.

In general, the quasi-cleavage facets are formed at or near the basal plane, which reflects the preference of dwell fatigue-crack initiation. The facets-size distributions of all LCDF specimens under different σ_p have been counted and compared with the corresponding lamellar and equiaxed α_p grains size, as shown in Fig. 9. The average size of facets initiated at the lamellar α_p is about 11.2 μm, and the width of the lamellar α_p is only 3.3 μm (Fig. 9a). The average size of equiaxed facets is about 7.3 μm, which is a little larger than that of equiaxed α_p grains (6.2 μm). It indicated that the facets tend to be formed at the lamellar α_p clusters and equiaxed grains with larger sizes. It is believed that larger grains size supplies longer effective slip lengths, inducing more dislocation pileups and resulting in stronger local stress concentrations at grain boundaries, which promotes crack nucleation and formation of facets. It should be noted that this study actually only qualitatively analyzes the preference of facets formation. Since the facets size counted in this study is the projection of the three-dimensional facets on the two-dimensional micrograph. Hence, the real facets size is larger than the statistical value. This preference for the formation of facets is consistent with the results obtained by Prasad *et al.* [40] using the tilted SEM technique to calculate the actual size of the facets.

The EBSD analysis of the PM Ti-6Al-4V perpendicular to the loading direction

was shown in Fig. 10. It can be seen that there is a soft-hard grain pair that conforms to the binary model of the stress redistribution proposed by Bache *et al.* [3, 14]. As known, the elastic modulus varies greatly with the crystallographic orientation for the hexagonal-close-packed (hcp) metals [41]. The grain whose c-axis is almost parallel to the loading direction is defined as the hard grains (indicated by red hexagonal prisms in Fig. 9b). The grain whose c-axis is approximately perpendicular to the loading direction is defined as the soft grain (indicated by blue hexagonal prisms in Fig. 9b). Additionally, a cluster composed of several lamellar α_p grains with the same near (0001) orientation was also found in Fig. 9a, which means that the interface of these lamellar clusters is the upper limit of the slip length due to the ease of slip transmission between grains with similar orientations. Therefore, the lamellar clusters can be considered as a large hard grain. The stress redistribution model proposes that the stress redistribution between the soft-hard grain pair leads the hard grain to be subjected to a greater stress due to the overall strain compatibility of the material, thereby crack nucleation and propagation. However, the role of the dwell time in LCDF is not explained in this model. Recent experiments [42, 43] and numerical calculations [44, 45] have proved that this internal stress evolution will lead to creep in soft grains and gradually result in the stress redistribution, which yields the time-dependent dwell effect. Xu *et al*. [46] proved that the prism slip in soft grains leads to dislocation accumulation at the interface of soft and hard grains, which results in dislocation nucleation on the basal plane of adjacent hard grains. Relevant evidence was also found based on the TEM image of the failed LCDF specimens in this study.

Figure 11a shows the case of lamellar α_p grains, it can be seen that there are a large number of dislocations in the soft grain, and a serious dislocation pile-up is formed at the grain boundary. The equiaxed α_p grains in Fig. 11b also exhibit a similar result.

The EBSD analysis of the failed LCDF specimen adjacent to the fracture surface along the loading direction was shown in Fig. 12a. Hexagonal lattice overlays were added to the broken grains to show their crystal orientations. The basal and prism planes of these hexagonal lattices are not perpendicular to the loading axis, but at a certain angle of ???. Moreover, the basal and prism plane traces were depicted for these grains. The fracture traces of the grains are roughly aligned with the basal and prism plane traces, showing a qualitative correspondence. The Schmid factor images of the basal and prism slip systems were shown in Figs. 12(b,c), respectively. The crystal orientation of grains near the fracture path are close to the favorable slip direction of the basal or prism slip, and the corresponding Schmid factors are at a high level. This trend indicates that the microcracks gradually growing and merging to form macroscopic main cracks after the initiation at the basal plane is carried out along the path composed of grains whose crystal orientations are easier to activate basal or prism slip systems.

The mechanistic schematic of dwell-fatigue crack initiation and propagation was illustrated in Fig. 13. It can be described in three stages: (I) Firstly, local creep deformation occurs in the soft grains, resulting in the stress redistribution to the hard grains. The prism slip in soft grains causes the dislocation pileup at grain boundaries, which causes the local stress concentration. Under the action of the above two, the

dislocation density in the hard grains is higher, and the basal slip band is driven to cause crack nucleation (Fig. 13a). (II) Secondly, with increasing cycling, dwell promotes the accumulation of the cyclic creep in soft grains and the local stress concentration. Hard grains with larger sizes are more likely to reach the critical conditions and form microcracks at the basal planes. If the reverse stress is introduced, the reverse slip activity will release the dislocation pileup at the boundaries of hard grains to a certain extent, thereby reducing the strength of the local stress concentration and prolonging the N_{LCDF}. (III) Finally, microcracks grow and merge to form macroscopic main cracks, and then propagate along grains with better basal or prism orientation until failure (Fig. 13c).

The initial microstructure of as-HIPed Ti-6Al-4V powder compacts used in this study has a very high volume fraction of the α phase (94%), which has been shown to lead to a lower N_{LCDF} [35]. In addition, the hard-oriented lamellar clusters have a larger size, which is conducive to the initiation of cracks under LCDF. Eliminating this special microstructure configuration may be beneficial for improving the dwell-fatigue property. Our previous work has shown that the high-cycle fatigue property of powder titanium alloys can be significantly improved by adjusting the HIP process to achieve nearly full globularization of lamellar microstructures [28]. The dwell-fatigue property of PM titanium alloys may be improved by tailoring the microstructure through HIP and heat treatment processes, which will be investigated in the future work.

5. Conclusions

In the present work, the dwell-fatigue effect of as-HIPed Ti-6Al-4V powder compacts under different loading conditions was firstly investigated, and the fatigue damage mechanism and the crack-initiation and propagation were discussed. The main conclusions can be drawn as follows:

(1). Under the normalized loading conditions, the N_{LCDF} of PM Ti-6Al-4V alloys is significantly lower than that of N_{LCF}, showing strong sensitivity to dwell effects. The dwell debit of PM Ti-6Al-4V alloys is similar to or even weaker than that of wrought alloys, which may be attributed to the better microstructure homogeneity.

(2). The dwell acts on the whole stage of crack initiation and propagation. Compared with LCF, the dwell tends to induce multiple crack-initiation sites and accelerates crack propagation, and significantly aggravates the degree of material damage under LCDF.

(3). The σ_p and R have significant effects on the fatigue life and dwell-fatigue damage mechanism. Under the same dwell time, the increase of σ_p aggravates the damage of the material. The N_{LCDF} decreases with the increase of σ_p, but the dwell debit increases with the increase of σ_p. When R is positive, the N_{LCDF} increases with the increase of R. When R is negative, the introduction of a lower reverse stress makes the N_{LCDF} increase.

(4). The dwell-fatigue mechanism is closely related to the crystal orientation and size of special microstructure configurations. The hard-oriented lamellar α_p clusters in as-HIPed Ti-6Al-4V powder compacts are unfavorable to the fatigue life. Cracks tend to initiate in special microstructures configurations with larger sizes and propagate along

grains with a better basal or prism orientation. A crack-initiation and propagation model based on a soft-hard grain pair is used to describe the dwell-fatigue mechanism of as-HIPed Ti-6Al-4V powder compacts.

Declaration of Competing Interest

The authors declare that they have no known competing financial interests or personal relationships that could have appeared to influence the work reported in this paper.

Acknowledgments

- This work was supported by the National Natural Science Foundation of China (No. 52205407), the Natural Science Foundation of Shanxi Province, China (Nos. 202203021221072, 202203021212237), and the CAS Project for Young Scientists in Basic Research (YSBR-025). PKL very much appreciates the support of National Science Foundation (DMR-1611180, 1809640, and 2226508).

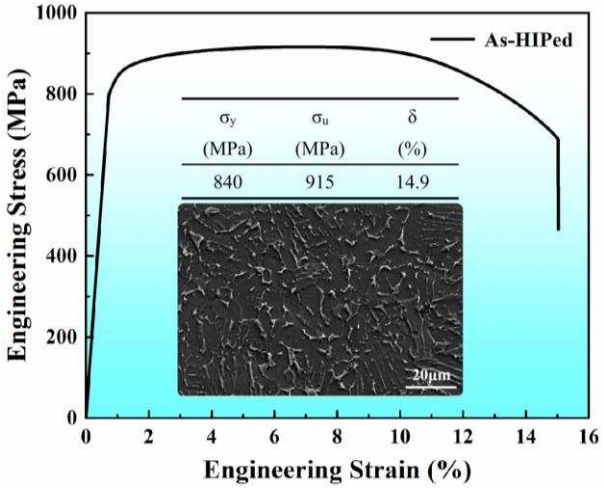

Fig. 1. The engineering stress-strain curve and microstructure of PM Ti-6Al-4V used

in the present work

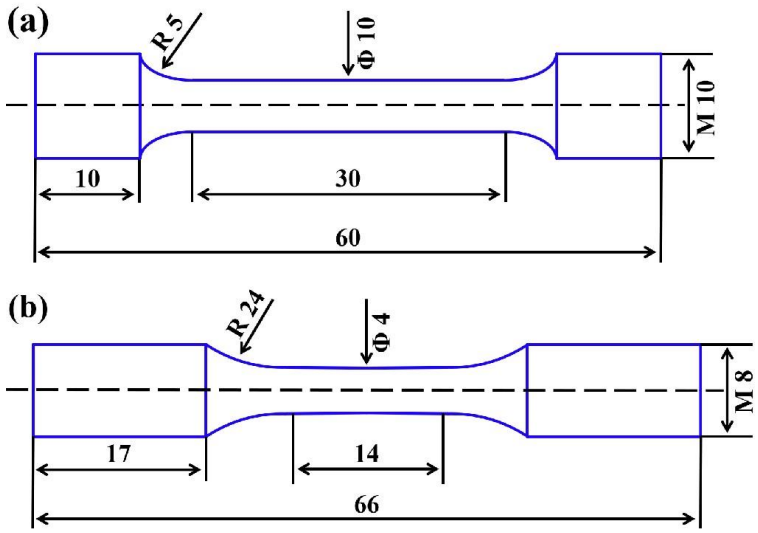

Fig. 2. Schematics showing the dimensions of (a) tensile tests and (b) fatigue tests specimens (unit: mm).

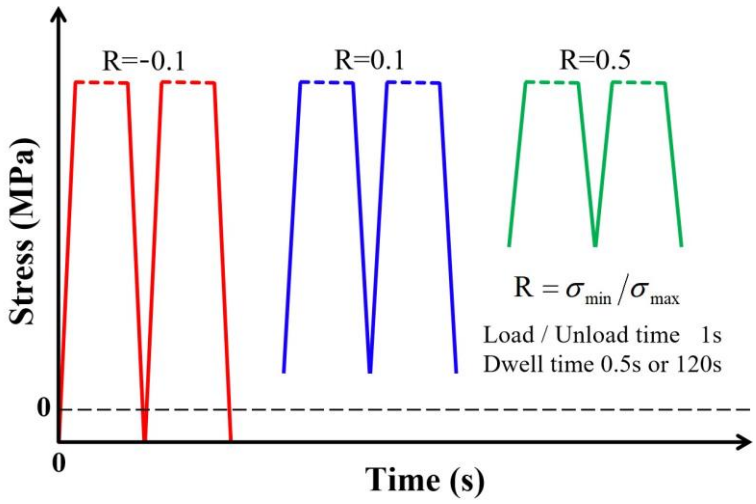

Fig. 3. Loading spectra for LCF and LCDF tests.

Table 1. Average dwell fatigue lives under different *R*.

σ_p (MPa)	*R*	Average N_{LCDF} (cycles)
825	- 0.1	874
	0.1	201
	0.5	1255

Table 2. Fatigue lives at different σ_p with R of 0.1.

σ_p (MPa)	N_{LCF} (cycles)	N_{LCDF} (cycles)	Dwell debit
775	4,156	1,811	2.1
	5,305	2,643	
800	3,862	571	6.4
	4,861	798	
825	1,282	137	7.9
	1,898	264	

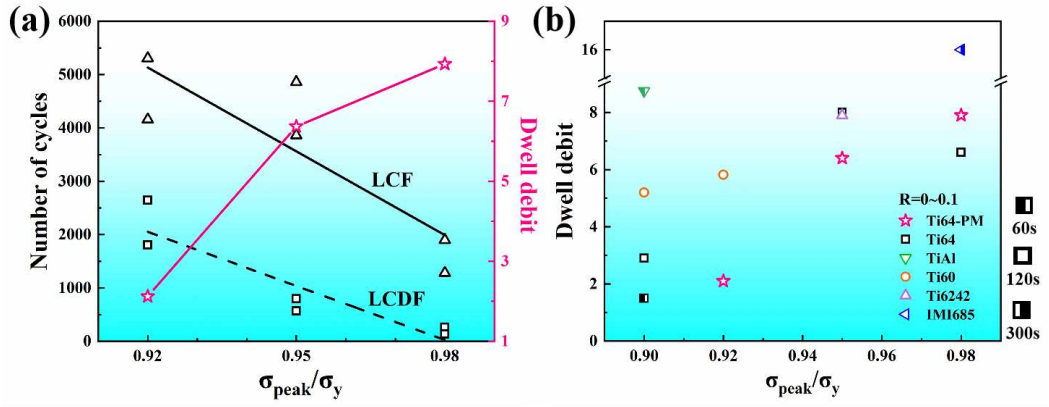

Fig. 4. Dwell effect under a normalized loading condition: (a) Fatigue lives and dwell debits of the PM Ti-6Al-4V with different σ_p; (b) Comparison of the dwell debits of the PM Ti-6Al-4V with other wrought titanium alloys, different color filling represents different dwell time.

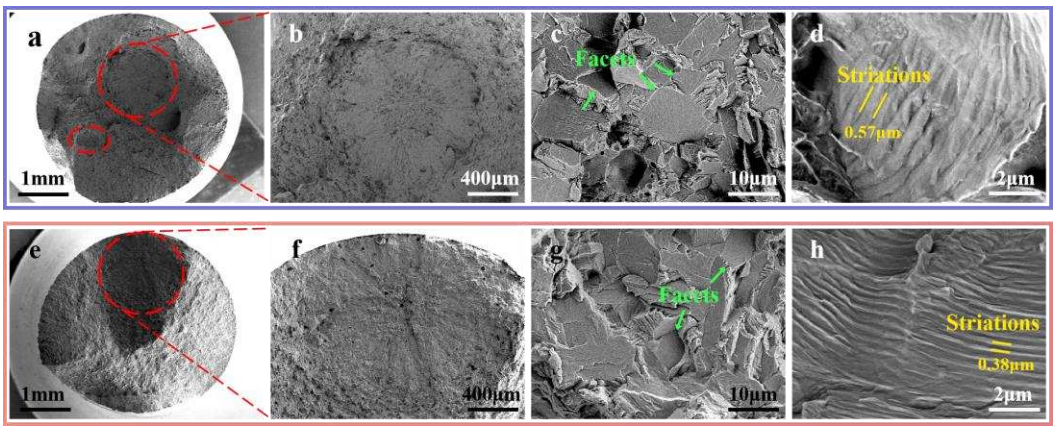

Fig. 5. SEM images presenting the fracture surfaces of the PM Ti-6Al-4V at σ_p = 775 MPa, R = 0.1: (a-d) N_{LCDF} = 1,811; (e-h) N_{LCF} = 5,305.

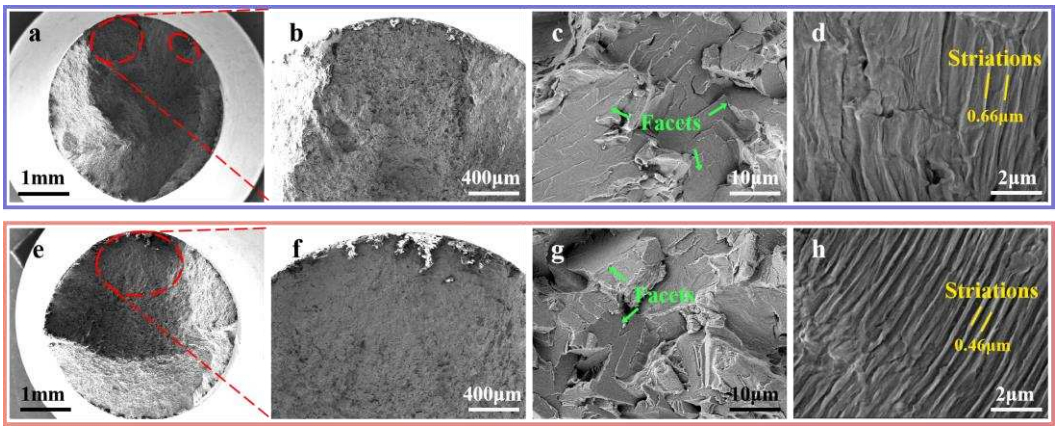

Fig. 6. SEM images presenting the fracture surfaces of the PM Ti-6Al-4V at σ_p = 800 MPa, R = 0.1: (a-d) N_{LCDF}=798; (e-h) N_{LCF}=3,862.

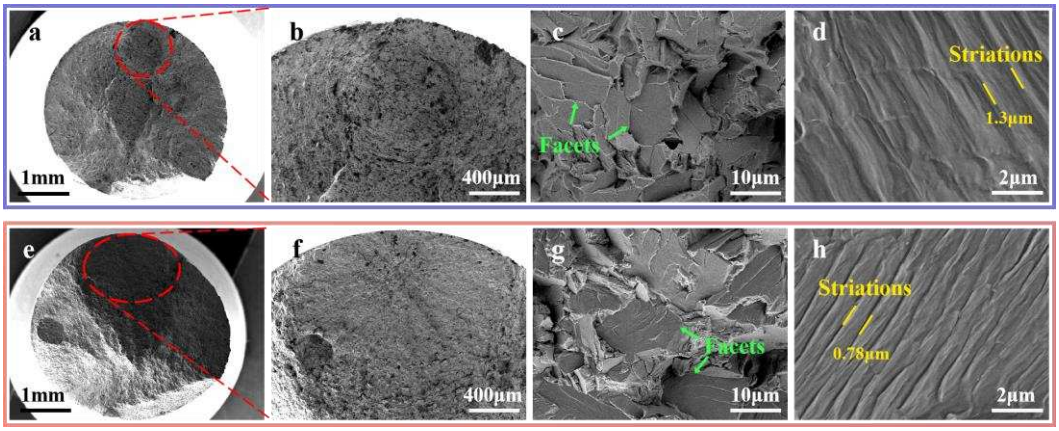

Fig. 7. SEM images presenting the fracture surfaces of the PM Ti-6Al-4V at σ_p = 825 MPa, R = 0.1: (a-d) N_{LCDF} = 264; (e-h) N_{LCF} = 1,898.

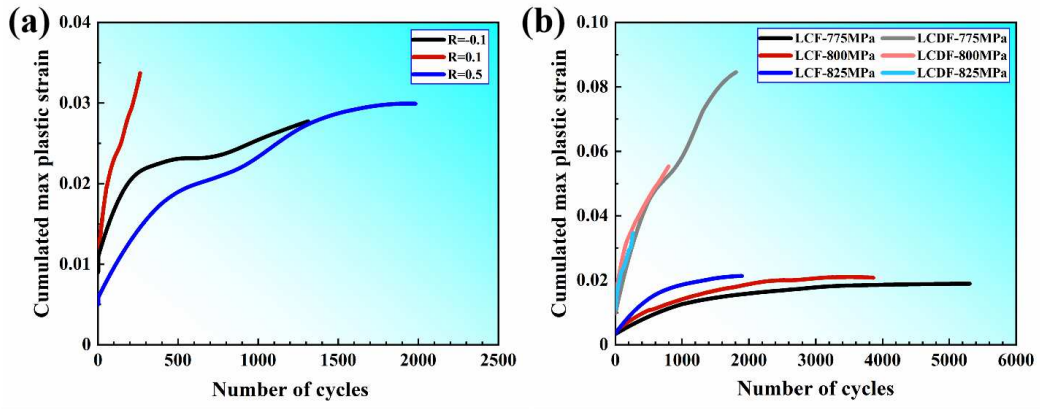

Fig.8. The cumulated max. plastic strain versus the number of cycles under different (a) R and (b) σ_p.

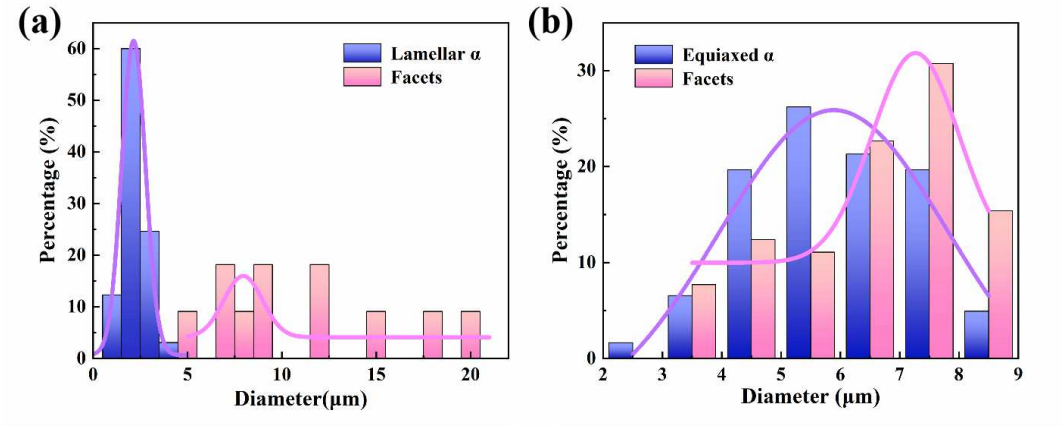

Fig. 9. The histograms of α grains sizes and corresponding facets size: (a) Lamellar α_p; (b) Equiaxed α_p.

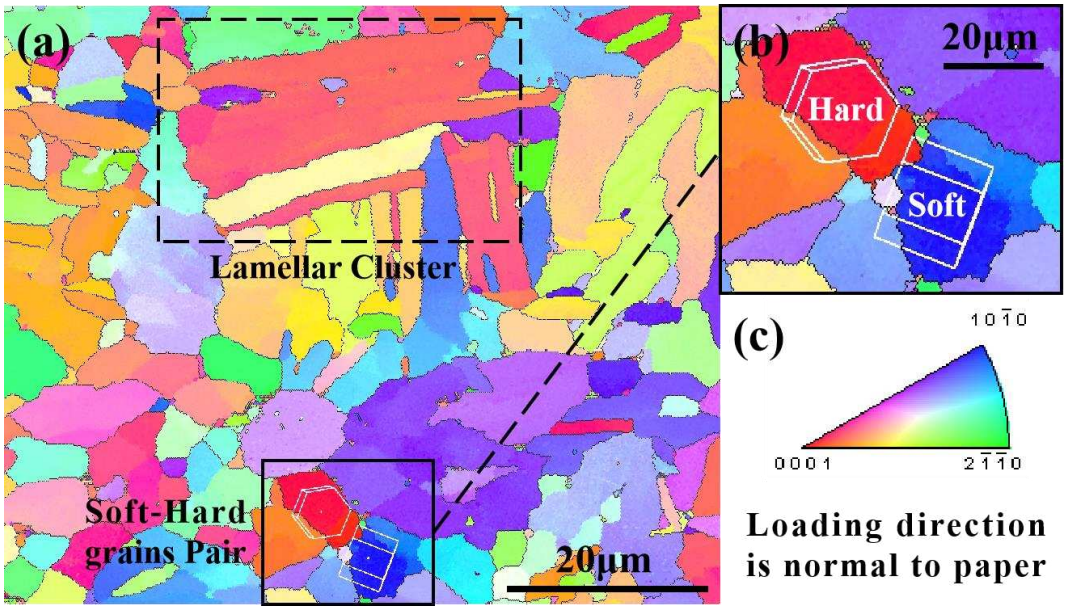

Fig. 10. Characterization of the as-received microstructure normal to the loading direction before LCDF tests: (a) EBSD images; (b) The enlarged image of soft-hard grain pair; (c) Orientation key.

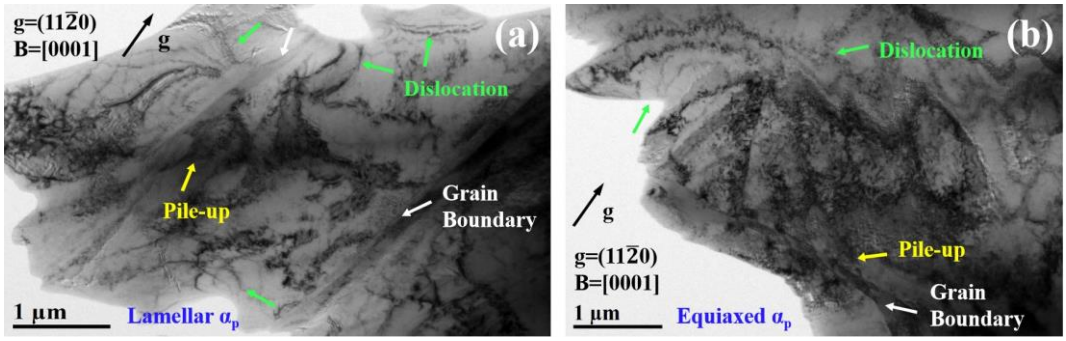

Fig. 11. TEM bright-filed images of the failure-fatigue specimen at σ_p = 825 MPa and R = 0.1, N_{LCDF}=137: (a) Lamellar α_p; (b) Equiaxed α_p.

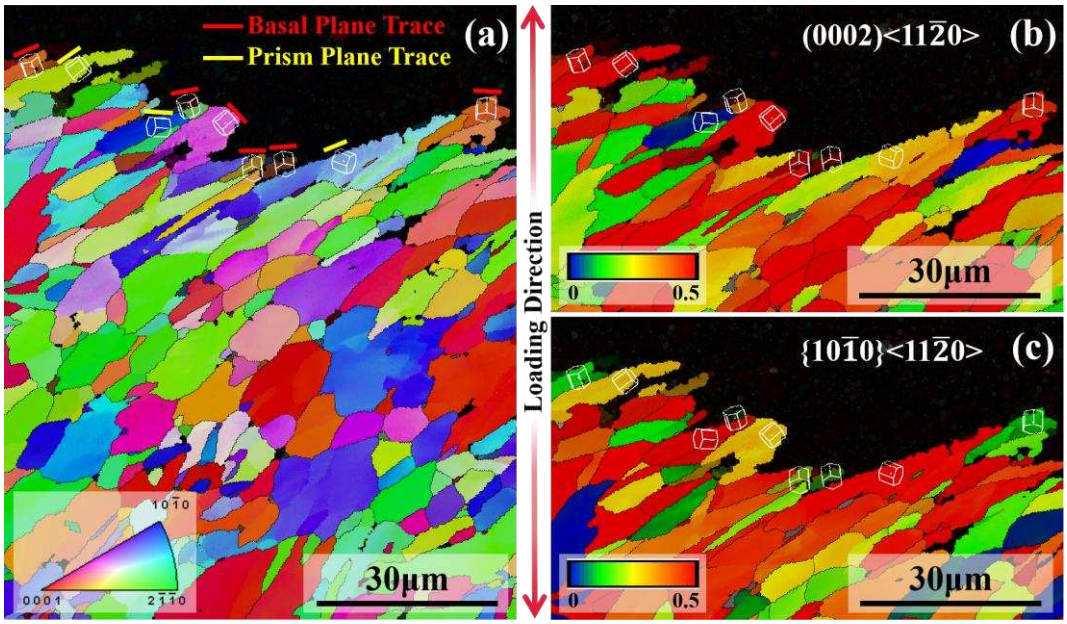

Fig. 12. Characterization of a longitudinal section near a crack-initiation site of failure Specimen at σ_p = 775 MPa and R = 0.1, N_{LCDF} = 1,811: (a) EBSD images; Schmid-factor diagram of (b) basal slip and (c) prism slip.

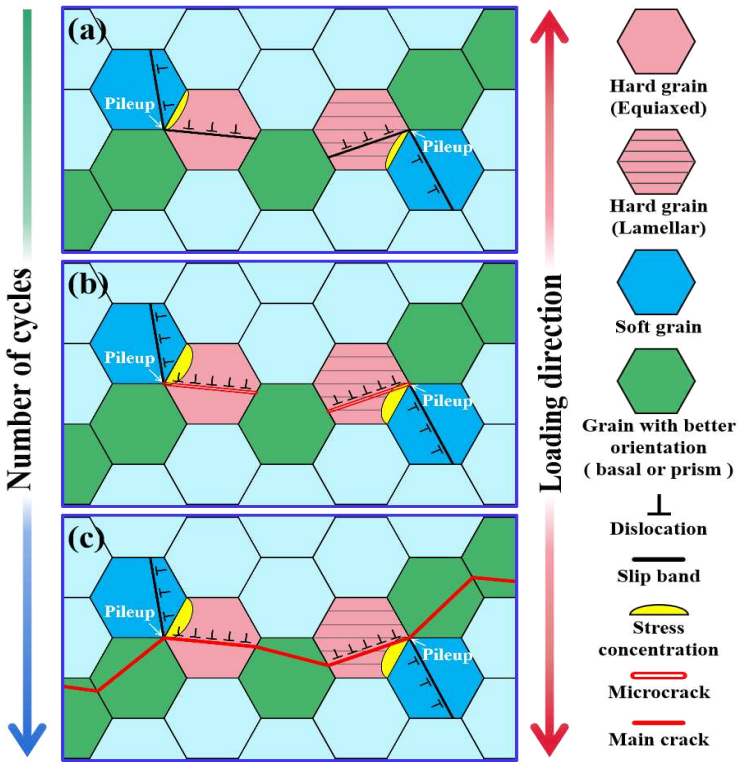

Fig. 13. Mechanistic schematic of dwell-fatigue crack initiation and propagation: (a) Crack nucleation; (b) Microcrack initiation; (c) Main crack propagation until failure.

References

[1] D. Banerjee, J.C. Williams, Perspectives on Titanium Science and Technology, Acta Materialia 61(3) (2013) 844-879.

[2] Suresh, S., Fatigue of Materials: Fatigue crack growth in brittle solids, 10.1017/CBO9780511806575(12) (1998) 408-432.

[3] M.R. Bache, A review of dwell sensitive fatigue in titanium alloys: the role of microstructure, texture and operating conditions, International Journal of Fatigue 25(9) (2003) 1079-1087.

[4] Z. Song, D.W. Hoeppner, Size effect on the fatigue behaviour of IMI 829 titanium alloy under dwell conditions, International Journal of Fatigue 11(2) (1989) 85-90.

[5] W.J. Evans, C.R. Gostelow, The effect of hold time on the fatigue properties of a β-processed titanium alloy, Metallurgical Transactions A 10(12) (1979) 1837-1846.

[6] F.P.E. Dunne, D. Rugg, A. Walker, Lengthscale-dependent, elastically anisotropic, physically-based hcp crystal plasticity: Application to cold-dwell fatigue in Ti alloys, International Journal of Plasticity 23(6) (2007) 1061-1083.

[7] F.P.E. Dunne, D. Rugg, On the mechanisms of fatigue facet nucleation in titanium alloys, Fatigue & Fracture of Engineering Materials & Structures 31(11) (2008) 949-958.

[8] C.J. Szczepanski, S.K. Jha, J. Jones, Microstructural Influences on Very-High-Cycle Fatigue-Crack Initiation in Ti-6246, Metallurgical&Materials Transactions A (2008).

[9] I. Bantounas, D. Dye, T.C. Lindley, The effect of grain orientation on fracture morphology during high-cycle fatigue of Ti–6Al–4V, Acta Materialia 57(12) (2009) 3584-3595.
[10] K.L. Biavant, S. Pommier, C. Prioul, Local texture and fatigue crack initiation in a Ti-6A1-4V titanium alloy, Fatigue & Fracture of Engineering Materials and Structures (6) (2002) 25.
[11] F. Bridier, P. Villechaise, J. Mendez, Slip and fatigue crack formation processes in an α/β titanium alloy in relation to crystallographic texture on different scales, Acta Materialia 56(15) (2008) 3951-3962.
[12] C. Lavogiez, S. Hémery, P. Villechaise, On the mechanism of fatigue and dwell-fatigue crack initiation in Ti-6Al-4V, Scripta Materialia 183 (2020) 117-121.
[13] S. Hémery, J.C. Stinville, F. Wang, M.A. Charpagne, M.G. Emigh, T.M. Pollock, V. Valle, Strain localization and fatigue crack formation at (0001) twist boundaries in titanium alloys, Acta Materialia 219 (2021) 117227.
[14] W.J. Evans, M.R. Bache, Dwell-sensitive fatigue under biaxial loads in the near-alpha titanium alloy IMI685, International Journal of Fatigue 16(7) (1994) 443-452.
[15] D. Ozturk, A.L. Pilchak, S. Ghosh, Experimentally validated dwell and cyclic fatigue crack nucleation model for α–titanium alloys, Scripta Materialia 127 (2017) 15-18.
[16] V. Hasija, S. Ghosh, M.J. Mills, D.S. Joseph, Deformation and creep modeling in polycrystalline Ti–6Al alloys, Acta Materialia 51(15) (2003) 4533-4549.
[17] S. Joseph, K. Joseph, T.C. Lindley, D. Dye, The role of dwell hold on the dislocation mechanisms of fatigue in a near alpha titanium alloy, International Journal of Plasticity 131 (2020) 102743.
[18] J. Qiu, Y. Ma, J. Lei, Y. Liu, A. Huang, D. Rugg, R. Yang, A Comparative Study on Dwell Fatigue of Ti-6Al-2Sn-4Zr-xMo (x = 2 to 6) Alloys on a Microstructure-Normalized Basis, Metallurgical and Materials Transactions A 45(13) (2014) 6075-6087.
[19] M.R. Bache, M. Cope, H.M. Davies, W.J. Evans, G. Harrison, Dwell sensitive fatigue in a near alpha titanium alloy at ambient temperature, International Journal of Fatigue 19(93) (1997) 83-88.
[20] R.H. Witt, A.L. Ferreri, TITANIUM NEAR NET SHAPE COMPONENTS FOR DEMANDING AIRFRAME APPLICATIONS Please have it in the lower case, 17 (1986) 55-62.
[21] F. Cao, K.S. Ravi Chandran, P. Kumar, P. Sun, Z. Zak Fang, M. Koopman, New Powder Metallurgical Approach to Achieve High Fatigue Strength in Ti-6Al-4V Alloy, Metallurgical and Materials Transactions A 47(5) (2016) 2335-2345.
[22] M. Cheng, B. Yu, R. Guo, X. Shi, L. Xu, J. Qiao, R. Yang, Electron beam welding of a novel near α high temperature titanium alloy powder compact: effect of post-welding heat treatment on tensile properties, Journal of Materials Research and Technology 10 (2021) 153-163.
[23] R.G. Lei XU, Jie WU, Zhengguan Lu, Rui Yang, Progress in Hot Isostatic Pressing Technology ofTitanium Alloy Powder, Acta Metall. Sin. in Chinese. 54 (2018) 1537–1552.
[24] K. Zhang, J. Mei, N. Wain, X. Wu, Effect of Hot-Isostatic-Pressing Parameters on the Microstructure and Properties of Powder Ti-6Al-4V Hot-Isostatically-Pressed Samples, Metallurgical and Materials Transactions A 41(4) (2010) 1033-1045.
[25] R. Guo, L. Xu, Z. Chen, Q. Wang, B.Y. Zong, R. Yang, Effect of powder surface state on microstructure and tensile properties of a novel near α-Ti alloy using hot isostatic pressing, Materials Science and Engineering: A 706 (2017) 57-63.
[26] C. Cai, B. Song, P. Xue, Q. Wei, C. Yan, Y. Shi, A novel near α-Ti alloy prepared by hot isostatic pressing: Microstructure evolution mechanism and high temperature tensile properties, Materials & Design 106 (2016) 371-379.

[27] M. Cheng, Z. Lu, J. Wu, R. Guo, J. Qiao, L. Xu, R. Yang, Effect of thermal induced porosity on high-cycle fatigue and very high-cycle fatigue behaviors of hot-isostatic-pressed Ti-6Al-4V powder components, Journal of Materials Science & Technology 98 (2022) 177-185.
[28] R.P. Guo, M. Cheng, C.J. Zhang, J.W. Qiao, C. Cai, Q.J. Wang, D.S. Xu, L. Xu, R. Yang, Y.S. Shi, P.K. Liaw, Achieving superior fatigue strength in a powder-metallurgy titanium alloy via in-situ globularization during hot isostatic pressing, Scripta Materialia 228 (2023) 115345.
[29] J. Sun, L. Wu, C. Sun, Effects of Notches and Defects on Dwell Fatigue Mechanism and Fatigue Life of Ti-6Al-4V ELI Alloy Used in Deep-Sea Submersibles, Journal of Marine Science and Engineering 9(8) (2021) 845.
[30] L. Xu, R. Guo, C. Bai, J. Lei, R. Yang, Effect of Hot Isostatic Pressing Conditions and Cooling Rate on Microstructure and Properties of Ti–6Al–4V Alloy from Atomized Powder, Journal of Materials Science & Technology 30(12) (2014) 1289-1295.
[31] C. Sun, Y. Li, R. Huang, L. Wang, J. Liu, L. Zhou, G. Duan, Crack initiation mechanism and fatigue life of titanium alloy Ti–6Al–2Sn–2Zr–3Mo-X: Effects of stress ratio and loading frequency, Materials Science and Engineering: A 798 (2020) 140265.
[32] C. Sun, Y. Li, K. Xu, B. Xu, Effects of intermittent loading time and stress ratio on dwell fatigue behavior of titanium alloy Ti-6Al-4V ELI used in deep-sea submersibles, Journal of Materials Science & Technology 77 (2021) 223-236.
[33] L. Yu, X. Song, L. You, Z. Jiao, H. Yu, Effect of dwell time on creep-fatigue life of a high-Nb TiAl alloy at 750°C, Scripta Materialia 109 (2015) 61-63.
[34] L. Yang, J. Liu, J. Tan, Z. Chen, Q. Wang, R. Yang, Dwell and Normal Cyclic Fatigue Behaviours of Ti60 Alloy, Journal of Materials Science & Technology 30(7) (2014) 706-709.
[35] L.R. Zeng, L.M. Lei, X.M. Luo, G.P. Zhang, Toward an understanding of dwell fatigue damage mechanism of bimodal Ti-6Al-4V alloys, Journal of Materials Science & Technology 108 (2022) 244-255.
[36] C. Huang, Y. Zhao, S. Xin, W. Zhou, Q. Li, W. Zeng, C. Tan, High cycle fatigue behavior of Ti–5Al–5Mo–5V–3Cr–1Zr titanium alloy with bimodal microstructure, Journal of Alloys and Compounds 695 (2017) 1966-1975.
[37] J.C. Williams, R.G. Baggerly, N.E. Paton, Deformation behavior of HCP Ti-Al alloy single crystals, Metallurgical & Materials Transactions A 33(13) (2002) 837-850.
[38] C. Liu, R. Thomas, T. Sun, J. Donoghue, X. Zhang, T.L. Burnett, J.Q. da Fonseca, M. Preuss, Multi-dimensional study of the effect of early slip activity on fatigue crack initiation in a near-α titanium alloy, Acta Materialia 233 (2022) 117967.
[39] J. Fan, W. Zhang, B. Li, K. Li, Y. Wang, P. Jiang, C. Wang, X. Xue, H. Kou, J. Li, Crystallographic analysis of slip system activation in bimodal Ti–6Al–3Nb–2Zr–1Mo alloy under various dwell-fatigue loadings, Materials Science and Engineering: A 865 (2023) 144610.
[40] K. Prasad, R. Sarkar, V. Singh, P. Ghosal, A. Bhattacharjee, H. Gokhale, On the probabilistic assessment of variability in fatigue life in a near α titanium alloy Timetal 834: Crystallography of fatigue crack initiating facets, Acta Materialia 218 (2021) 117214.
[41] ZARKADES, A., The Science, Technology and Application of Titanium || ELASTICITY OF TITANIUM SHEET ALLOYS, (1970) 933-941.
[42] M.R. Bache, F.P.E. Dunne, C. Madrigal, Experimental and crystal plasticity studies of deformation and crack nucleation in a titanium alloy, The Journal of Strain Analysis for Engineering Design 45(5) (2009) 391-399.

[43] M.J.M. V. Sinha, J.C. Williams, Crystallography of Fracture Facets in aNear-Alpha Titanium Alloy, METALLURGICAL AND MATERIALS TRANSACTIONSA 37A(June) (2006) 2006-2015.
[44] G. Venkatramani, S. Ghosh, M. Mills, A size-dependent crystal plasticity finite-element model for creep and load shedding in polycrystalline titanium alloys, Acta Materialia 55(11) (2007) 3971-3986.
[45] M. Anahid, M.K. Samal, S. Ghosh, Dwell fatigue crack nucleation model based on crystal plasticity finite element simulations of polycrystalline titanium alloys, Journal of the Mechanics & Physics of Solids 59(10) (2011) 2157-2176.
[46] Y. Xu, S. Joseph, P. Karamched, K. Fox, D. Rugg, F.P.E. Dunne, D. Dye, Predicting dwell fatigue life in titanium alloys using modelling and experiment, Nature Communications 11(1) (2020) 5868.